

The Low-Level Structure of African Easterly Waves in 1995

IOANNIS PYTHAROULIS AND CHRIS THORNCROFT

Department of Meteorology, University of Reading, Reading, United Kingdom

(Manuscript received 20 February 1998, in final form 1 July 1998)

ABSTRACT

The existence of African easterly waves (AEWs) north of the African easterly jet (AEJ) core with maximum amplitude at low levels has been confirmed and clarified using radiosonde data and the U.K. Meteorological Office global model analysis from the hurricane season of 1995. At Bamako (12.5°N, 8.0°W) the AEWs were characterized mainly by maximum amplitudes at the level of the AEJ (around 700 mb), whereas at Dakar (14.7°N, 17.5°W) the waves were characterized by maxima between 850 and 950 mb. The low-level waves to the north of the AEJ arise in association with baroclinic interactions between the negative meridional potential vorticity (PV) gradients in the jet core and the positive low-level gradient of potential temperature, θ , enhanced by the presence of low-static-stability air north of the AEJ. These waves follow the positive meridional θ gradients over northern Africa in contrast to the jet-level AEWs that follow the meridional PV gradients at the level of the AEJ. Cross-correlation analysis shows that there is strong coherence between the low-level AEWs and the well-known cold core AEWs that propagate south of the jet, confirming that AEWs are associated with a combined barotropic–baroclinic instability mechanism.

1. Introduction

It is well known that during Northern Hemisphere summer, synoptic-scale disturbances form in the easterlies over tropical northern Africa. These disturbances known as African easterly waves (AEWs) typically have periods of 3–5 days, a wavelength of about 2000–4000 km, and propagate westward with a mean speed of about 6° – 7° long day⁻¹ (7 – 9 m s⁻¹) at a mean latitude of 11°N over land and 12°N over the ocean (e.g., Reed et al. 1977). They also propagate across the tropical North Atlantic Ocean often reaching the Caribbean and even the eastern Pacific. These waves have been recognized to contribute to the tropical cyclogenesis not only in the Atlantic and the Caribbean (Riehl 1954; Frank 1970; Landsea 1993) but also in the eastern Pacific basin (Avila and Pasch 1995).

Much has been written about the structure of the AEWs based on both observational and modeling studies (e.g., Burpee 1974; Reed et al. 1977; Thorncroft and Hoskins 1994a; Paradis et al. 1995). Most have emphasized the easterly wave structure south of the African easterly jet (AEJ) at the jet level. The present study, however, will show that typically AEWs are also characterized by marked low-level anomalies to the north

of the AEJ. This aspect of AEWs has generally been ignored in recent work although it is clearly present in some previous studies. Carlson (1969b) using 2000-ft and 10 000-ft streamline charts for 1968 found a low-level relatively cloud-free vortex located at about 20°N and suggested that it is produced indirectly by the wave's circulation, implying that it is linked to the primary (700 mb) wave. Burpee (1974) using surface observations and upper-air data for the summers of 1968 and 1969 found that the average amplitude of the 1200 UTC surface meridional wind and surface pressure calculated from power spectra at periods of 3.6–5.7 days have maximum values at about 20°N (i.e., north of the AEJ). Furthermore, streamline analysis of composite data revealed the existence of two cyclonic centers (on either side of the jet) and it was suggested that the northern one was associated with the semipermanent east–west-oriented line of minimum surface pressure near 20°N, while the southern one was related to the rainy zone (at latitudes near 10°N). Reed et al. (1977) presented a composite analysis of the Global Atlantic Tropical Experiment (GATE) easterly waves and also found two circulation centers at the surface. One center was located below the 700-mb wave (which propagated at about 11°N) and the other was located at about 20°N again north of the AEJ. Dual centers appeared to occur mainly over the land.

More recently, Reed et al. (1988a) using European Centre for Medium-Range Weather Forecasts data from 1985 found that the AEWs propagated in two tracks over the land (on either side of the jet) while over the

Corresponding author address: Chris Thorncroft, Department of Meteorology, University of Reading, Earley Gate, P.O. BOX 243, Reading RG6 6BB, United Kingdom.
E-mail: C.D.Thorncroft@reading.ac.uk

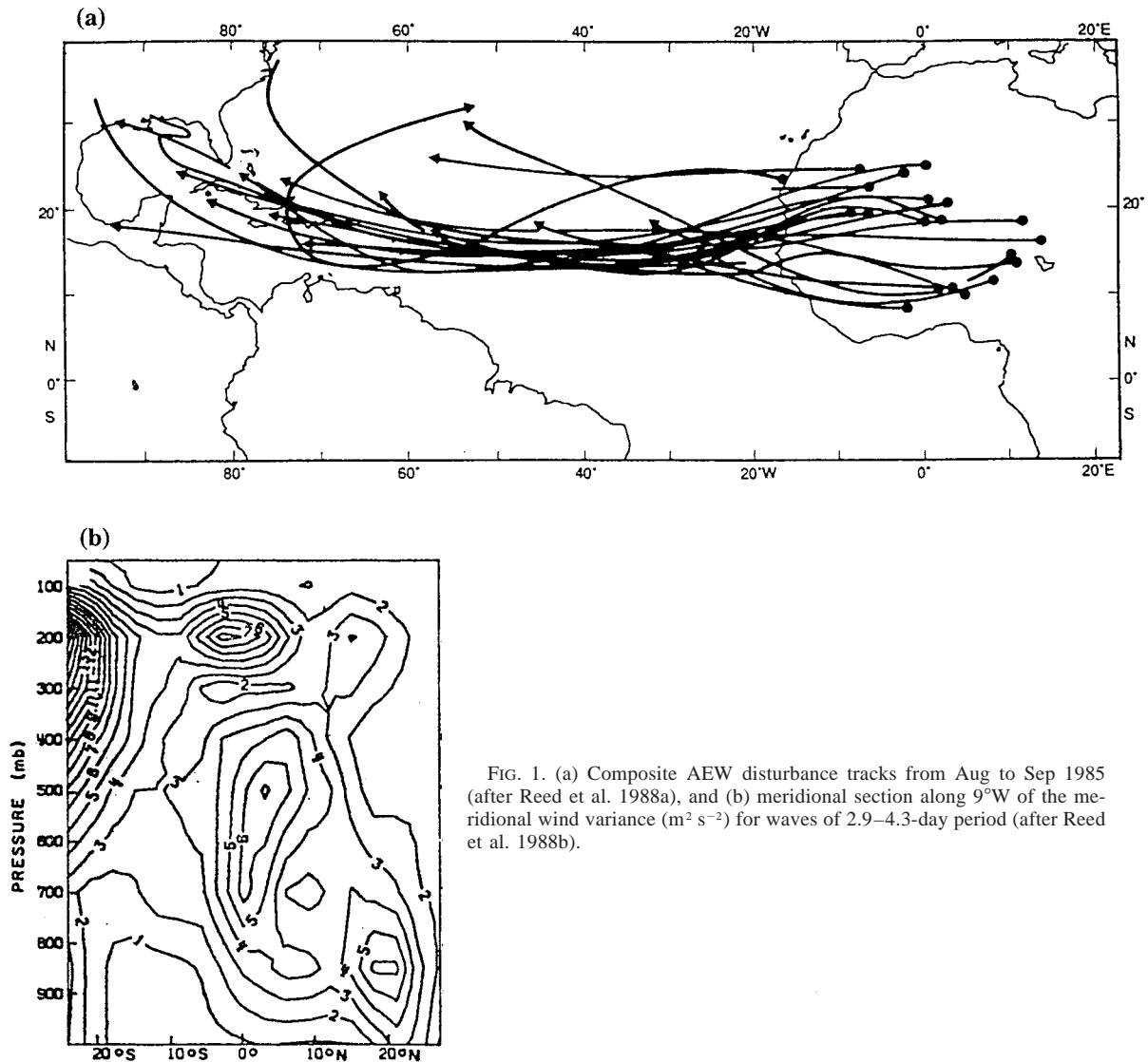


FIG. 1. (a) Composite AEW disturbance tracks from Aug to Sep 1985 (after Reed et al. 1988a), and (b) meridional section along 9°W of the meridional wind variance ($\text{m}^2 \text{s}^{-2}$) for waves of 2.9–4.3-day period (after Reed et al. 1988b).

ocean they merged and moved at about 15°N (Fig. 1a). This work seemed to suggest that two separate types of AEWs existed north and south of the AEJ. Reed et al. (1988b) as part of the same study showed that large values of meridional wind variance (associated with waves of 2.9–4.3-day periods) existed at low levels north of the mean latitude of the AEJ, while south of the jet the maximum meridional wind variance was observed at the jet level (Fig. 1b). Since the tracks in Fig. 1a were mainly based on 700- and 850-mb data, it can be seen in Fig. 1b that at 850 mb the waves of both tracks could be seen. Similarly, Nitta and Takayabu (1985) found two different paths of AEWs over the land but with the southern one extending much farther into the Atlantic. No track merger appeared in their study and coherence analysis indicated that the waves following the two paths were coupled. On the other hand,

Miyakoda et al. (1982) using GATE data only found high values of transient relative vorticity near 700 mb south of the AEJ. From this brief examination of the literature it is not clear whether the AEWs are systems with two circulation centers at low levels but with one strong vorticity maximum at 700 mb south of the AEJ or if there are two different kinds of AEWs growing on either side of the jet.

From a theoretical perspective, the AEJ has been shown to satisfy the Charney and Stern (1962) instability criterion (Burpee 1972)—the necessary condition for barotropic and baroclinic instability. Following Thorncroft and Hoskins (1994a), Fig. 2 is a schematic of the meridional gradients of Ertel potential vorticity ($PV; \partial\bar{q}/\partial y$) over North Africa versus latitude and height. The surface meridional gradient of potential temperature ($\partial\bar{\theta}/\partial y$) is also depicted in the figure. Two possible

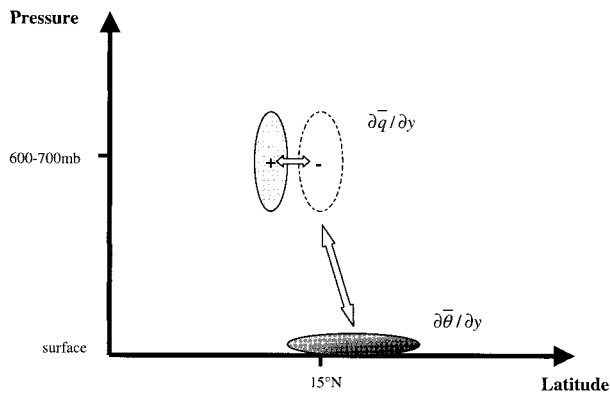


FIG. 2. Schematic of the meridional gradients of PV ($\partial\bar{q}/\partial y$), the low-level meridional gradient of potential temperature ($\partial\bar{\theta}/\partial y$), and their interactions (indicated by the arrows) over North Africa. The plus (+) and minus (-) signs denote positive and negative values, respectively.

strongly interacting pairs of PV gradients exist. These are the interactions between the negative $\partial\bar{q}/\partial y$ in the jet core with (a) the positive $\partial\bar{q}/\partial y$ on the equatorward flank of the jet, and (b) the positive $\partial\bar{\theta}/\partial y$ at the surface. The instability criterion is also satisfied with the positive $\partial\bar{q}/\partial y$ above and below the jet and the negative $\partial\bar{q}/\partial y$ in the jet, but the instability is expected to be much weaker there because the PV gradients are much weaker above and below the jet (Thorncroft and Hoskins 1994a). Moreover, Thorncroft and Hoskins (1994a) showed that the Fjörtoft condition for instability, which requires the mean zonal wind to be positively correlated with the $\partial\bar{q}/\partial y$ and the surface $\partial\bar{\theta}/\partial y$ gradients, is indeed satisfied.

A normal mode study of an idealized AEJ with an initial PV structure similar to that implied by Fig. 2 showed that both interactions occur (Thorncroft and Hoskins 1994a). Maximum eddy kinetic energy was found north and south of the jet near the AEJ level and also in the region of the maximum $\partial\bar{\theta}/\partial y$ near the surface. Thorncroft (1995) found that the AEW disturbances are expected to attain larger amplitudes if they evolve in areas with low N^2 (Brunt-Väisälä frequency) such as the Saharan Desert environment due to increased baroclinic instability. Similarly, Chang (1993) found that the low-static-stability environment to the north of the AEJ is favorable for the growth of disturbances with AEW characteristics. Thorncroft and Hoskins (1994b) examined the nonlinear life cycle of the AEWs in order to simulate them when they reach the West African coast and found large amplitudes to develop at low levels in the regions of strong $\partial\bar{\theta}/\partial y$.

Generally, little attention has been given to the waves that follow the northern track. This may be due to lack of observations in the Saharan Desert region or because they are generally very dry and do not affect the rainfall in the region. Alternatively it may be because their existence has not been clarified or understood. Indeed, the

need to clarify the relationship between the disturbances that follow the two tracks was admitted by Nitta and Takayabu (1985).

The aim of this paper is to provide further evidence for the existence of low-level AEW structures to the north of the AEJ that propagate over the sub-Saharan baroclinic zone, and to explore their relationship with the 700-mb waves that evolve in the rainy zone of Africa and the AEJ. This study is based on data from the summer and autumn of 1995. This particular year was chosen for analysis because it was an unusually active hurricane year (with 19 tropical storms in the Atlantic; 11 of them reaching hurricane strength) (Lawrence et al. 1998). Since it is generally accepted that AEWs play a crucial role in the tropical cyclogenesis in the Atlantic, this offered further motivation to examine the easterly waves in this year. Indeed, Pasch et al. (1998) showed that 90% of the Atlantic tropical depressions of 1995 were of African origin while all the hurricanes of that season were formerly AEWs. Section 2 will describe the data used and the analysis techniques employed. The possible role of the mean PV and θ gradients will be discussed in section 3. Examination of the structure and the characteristics of these waves will be done in section 4 and some inferences on their energetics are going to be made. Finally, the conclusions from this work will be presented in section 5.

2. Data and methods

The data used in this study were radiosonde data from May to October 1995 and analysis data from the global version of the United Kingdom Meteorological Office (UKMO) Unified Model from June to October 1995. Meteosat infrared satellite images were also used (but not shown here) to examine the strength of the convective activity associated with the waves. The radiosonde analysis was done for Dakar (14.7°N, 17.5°W) and Bamako (12.5°N, 8.0°W); see Fig. 5 for the location of each station. These two stations were chosen not only because they provide data with good vertical and temporal resolution (compared with the nearby stations) but also because they are located inside the main area of AEW development [as indicated by Albignat and Reed (1980) and consistent with the model analysis presented in section 4]. The radiosonde data from Dakar consisted of ascents made twice daily, at 1100 and 2300 UTC, while at Bamako data were available only for 1100 UTC. The percentage of valid points (i.e., at the above standard times) was greater than 80% of the maximum possible number of points for both stations. Moreover, Reed et al. (1988a) showed in Fig. 1a that the waves that follow the northern track pass close to Dakar when they leave the West African coast while the waves that follow the southern track pass closer and generally south of Bamako. Dakar is not the most ideal station to study the waves that follow the northern track but it is the station with the best data in the region.

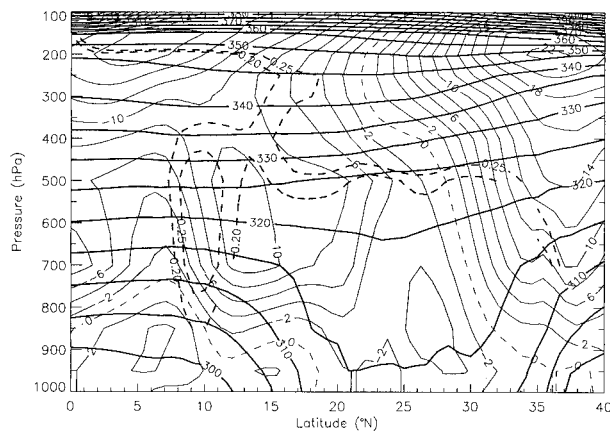


FIG. 3. Meridional section of potential temperature at 5°E (bold solid lines) with zonal wind at 5.625°E (light solid) and Ertel PV (bold dashed) equal to 0.2 and 0.25 PVU at 5°E overplotted. All graphs are averaged over all times in Aug 1995. Contour interval = 5 K, 2 m s⁻¹, 0.05 PVU (1 PVU = 10⁻⁶ m² K s⁻¹ kg⁻¹). The shaded regions correspond to easterlies (UKMO analysis data).

Logarithmic interpolation in pressure was used to derive values at 50-mb intervals. Linear interpolation in time was applied in the case of one missing observation (using all the available data), while in the case of more than one consecutive missing point, the mean value of the whole (6 months) time series was used in order to have the least variance associated with these points. Bandpass filtering in time has been used to isolate those oscillations associated with AEWs. The characteristics of the Lanczos filter that was used are discussed in Duchon (1979).

Operational analysis data from the UKMO Unified Model were also used. The operational model is an atmosphere only, hydrostatic, primitive equation model. The variables are calculated on a 0.833° lat × 1.25° long Arakawa B grid. In the vertical a hybrid coordinate is used with higher resolution in the boundary layer. Nineteen model levels are used in total. More information for the configuration of the model can be found in Cullen (1993).

The model analysis consisted of gridpoint data from June to October 1995. These data were available four times per day (at 0000 UTC, 0600 UTC, 1200 UTC, and 1800 UTC).

When dealing with model analyses it must be recognized that data coverage over the northern African region is certainly not as good as in other areas (such as North America or Europe). In the region between the equator and 15°N and west of 25°E about 70 surface stations and 7 stations with radiosonde data were included in the UKMO analyses. Cloud-track winds were also included. North of 15°N the number of observations decreases dramatically as the Saharan desert is reached. Data from about 40 surface stations and 6 stations with radiosonde data as well as cloud track winds were used in the model analyses from the northern region (between 15° and 30°N and west of about 15°E). Generally, very few observations are available from the region east of about 20°E. In this study analyses are used alongside radiosonde data from two stations to give a larger-scale view of the AEWs.

3. The mean PV and θ structure over northern Africa and the Atlantic

AEWs arise through an instability of the opposite signed PV gradients and the low-level θ gradients (Fig. 2); the reversal of the meridional PV gradient on the southern flank of the AEJ core can be seen in the UKMO analysis for August 1995 (Figs. 3, 4). With this in mind, given that PV is conserved on isentropic surfaces in adiabatic and frictionless motions (Hoskins et al. 1985) and after an examination of Fig. 3, the 315 K surface was chosen to illustrate the mean PV since this surface transects the AEJ. This surface is at about 700 mb south of the jet (Fig. 3) and over the Atlantic, but it is very close to the ground (even reaching it in the warm part of the day) north of the jet. Figure 4 shows clearly the jet-level PV gradients discussed in section 1. On this isentropic surface, the positive PV gradients extend from the African continent to the Caribbean (Fig. 4),

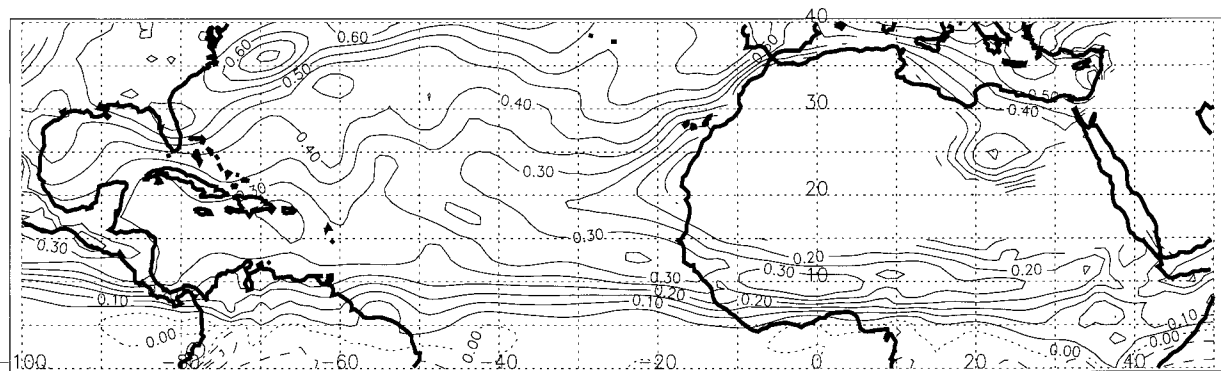


FIG. 4. Horizontal section of Ertel PV at 315 K for Aug 1995 (averaged over all times). Contour interval = 0.05 PVU (UKMO analysis data).

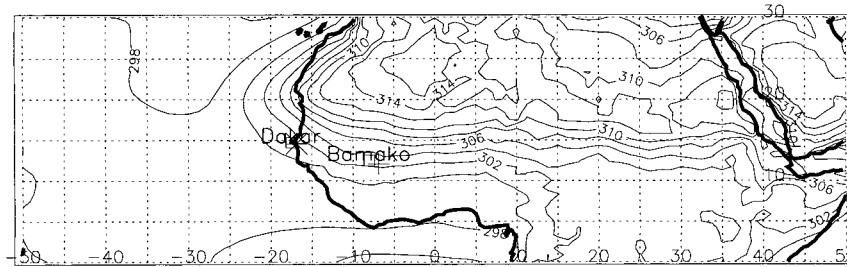


FIG. 5. Horizontal section of potential temperature at 950 mb for Aug 1995 (averaged over all times). Contour interval = 2 K. The location of Dakar, Bamako, and of the grid points with coordinates 14.583°N, 16.875°W (*) and 12.083°N, 6.875°W (+) are marked on the figure (UKMO analysis data).

and the AEWs that form and propagate south of the jet (near the jet level) would be expected to follow these gradients. An examination of the PV gradients on the 315 K surface in other months (not shown) indicated that the negative meridional PV gradients in the jet core were strongest in August. Molinari et al. (1997) in a study in the Caribbean noted that the magnitude of the negative PV gradient is related to the growth rate of a disturbance. Consistent with this and theoretical studies (e.g., Thorncroft and Hoskins 1994a) stronger AEWs would be expected to form in that month. If there is some relationship between tropical cyclogenesis and AEWs (cf. Riehl 1954; Frank 1970; Landsea 1993) and if all the other large-scale factors that affect tropical cyclogenesis (Landsea et al. 1994) were assumed to be the same throughout the season, August should have been the most active month of 1995. Consistent with this, 7 of the 19 North Atlantic tropical cyclones of 1995 formed in August, making it the most active month of that season.

At low levels strong θ gradients exist over land only (Fig. 5). The θ gradients extend from one side of northern Africa to the other and they appear to be stronger near the latitude of the AEJ and slightly to the north. An inspection of Figs. 3 and 5 shows that the dry static stability is very small in the region north of the jet (at low levels). This is associated with the high surface temperatures and a deep well-mixed layer especially over the Saharan Desert from about 17° to 33°N (see Thorncroft and Blackburn 1999). As discussed by Thorncroft (1995) the low static stability in the desert region to the north of the jet (Fig. 3) increases the interaction between the PV anomalies on the jet and the temperature anomalies at the ground. Consistent with the discussion above, large wave amplitudes are expected at both the jet level and the surface.

The zonally elongated θ gradients do not extend into the Atlantic but follow the West African coast toward the north (Fig. 5). Hence, while the 700-mb waves may be expected to move westward over the Atlantic following the zonally elongated PV gradients, it is not obvious what the low-level waves will do when they reach the coast. Some of them may continue northward

as neutral Rossby waves following the θ gradients (Fig. 5); others may continue westward as indicated by Nitta and Takayabu (1985), while others may move southward until they are located below the 700-mb maximum. In the second case the strong low-level winds would be expected to result in increased surface fluxes of moisture from the underlying ocean and an increase in boundary layer equivalent potential temperature (θ_e). The increased buoyancy of the low-level air may increase the likelihood of convection and a Wind Induced Surface Heat Exchange (WISHE) type development may be expected (Emanuel 1986). However, another important aspect of the low-level waves (to the north) is their dryness aloft. If convective activity erupts, the dryness of these waves aloft may cause strong downdrafts, stabilizing the air at low levels and inhibiting WISHE development. It is unclear how the convection will evolve in these waves and what impact this will have on the waves. Future work in this area is recommended. The third possibility is to have an interaction between the jet-level and low-level waves. In this case the 700-mb wave can “constructively interfere” with the low-level wave in order to strengthen the low-level winds (cf. Molinari et al. 1995), enhance the surface fluxes of moisture, and again trigger the WISHE mechanism.

4. The African easterly wave structures in 1995

a. Single point analysis

Radiosonde data analysis at Dakar and Bamako is now presented in order to examine the structure of the AEWs. Although the examination of the model analyses later provides a clearer insight of the waves, radiosonde data are presented to confirm the wave structures using real observations with no model bias.

1) POWER SPECTRA

Power spectrum analysis of the meridional wind time series at 700 and 950 mb (Fig. 6) indicates substantial power in the 2.5–6-day timescale. These two levels were

chosen because they are expected to reflect more clearly the AEWs at the jet level and low levels. Different features appear at the two stations. At Dakar (Fig. 6a) the strongest power associated with AEWs is at very low levels while at Bamako (Fig. 6b) the waves have a very strong signal at 700 mb where they exhibit a period of about 4.9 days. No strong AEW signal appears at 950 mb at Bamako. These results indicate that the easterly waves that pass from Dakar are dominated by a structure with maximum amplitude at low levels while mainly jet-level structures pass Bamako.

Our finding that the AEWs in 1995 exhibited periods between 2.5 and 6 days is consistent with studies based on data from other years. Burpee (1972) found strong variance of the meridional wind at Dakar at about 3–5 days at 700 mb. Viltard and De Felice (1979) using radiosonde data from Dakar found strong spectral energy associated with AEWs with periods between 3.2 and 4 days (with the strongest signal at about 700–800 mb). Moreover, Albignat and Reed (1980) found a spectral peak in the 850-mb meridional wind time series at Dakar lying between 2.5 and 5 days.

2) KINEMATIC STRUCTURE AND CONVECTIVE ACTIVITY

The radiosonde data analysis at Dakar and Bamako in 1995 and particularly time–height plots of meridional wind show the AEWs that passed each station. Although the analysis of the unfiltered radiosonde data provides good insight of the structure of the waves, a clearer picture is seen if the flow not associated with the waves is removed.

Bandpass filtering was therefore performed at the 2.5–6-day timescale to make the analysis clearer. Figures 7a,b are time–height plots of the 2.5–6-day filtered meridional wind and they depict the vertical structure of the waves that passed Dakar and Bamako in July 1995. This month was chosen because, in this year, it was one of the months that the AEWs were more clearly defined at these stations. The most interesting point of Fig. 7 is that strong waves appear at low levels at Dakar while the strongest part of the waves at Bamako appears to be nearer the AEJ (which had a maximum at about 600 mb in July), consistent with Fig. 6.

The vertical distribution of the mean strength of the meridional wind fluctuations in the 2.5–6-day timescale is further illustrated in Fig. 8. In agreement with the above, the maximum wave energy at Dakar is observed at very low levels (especially in July) and certainly below the core of the AEJ. On the other hand, a double maximum appears at Bamako and the strongest wave activity is observed at 850 and 700 mb (close to the AEJ maximum). There is a considerable intraseasonal variation in the nature of the AEWs at each station. The waves appeared to be well developed in July at both stations. At Dakar the waves were also strong in August

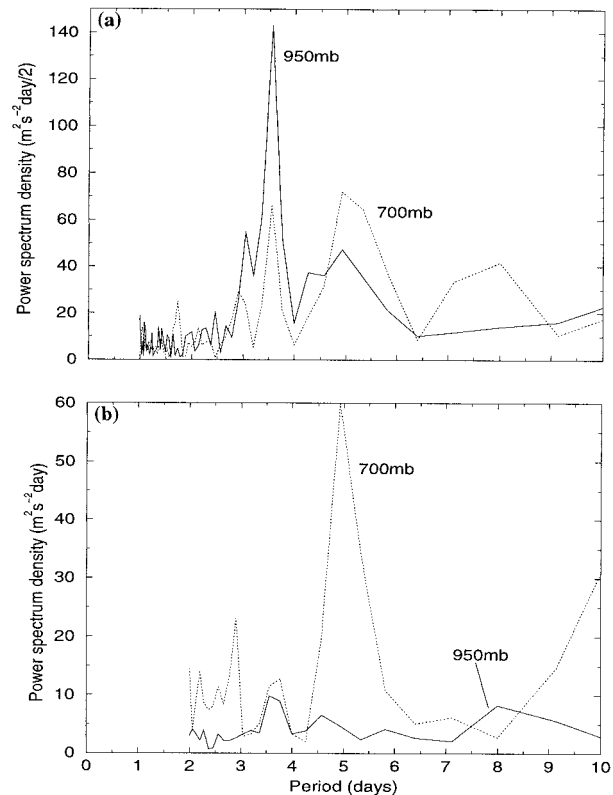


FIG. 6. Power spectrum density vs period of the meridional wind time series from May to Oct 1995 at (a) Dakar, (b) Bamako. Solid line: 950 mb, dotted line: 700 mb (radiosonde data).

especially at low levels and very weak in September, while at Bamako the second strongest month was September and August was a generally weak month. These differences imply that waves of different nature passed from the two stations. It should be noted that the results from each station may not reflect the actual maxima of the waves since the AEW maximum may not always pass from these stations and the results are influenced by the relative position of the AEJ to the station.

It is expected that the AEWs that grow on the southern flank of the jet (in the rainy zone of Africa) will be associated with stronger convective activity than the low-level waves that form in the northern flank of the jet (i.e., on the southern edge of the Sahara Desert). This has been examined through analysis of infrared satellite imagery. Time series of the number of pixels (derived from 3-hourly Meteosat infrared imagery in a $3^\circ \times 3^\circ$ box centered at each station) with temperature colder than a threshold value have been examined. The cloud-top temperature of -50°C was taken as the characteristic threshold value of deep convection in the region. Also, it must be mentioned that the pixel dimensions are $0.115^\circ \text{ lat} \times 0.123^\circ \text{ long}$. The mean number of pixels (per image) with temperature below -50°C (averaged from July to September 1995) was 27.3 and 51.2 and the standard deviation of the time

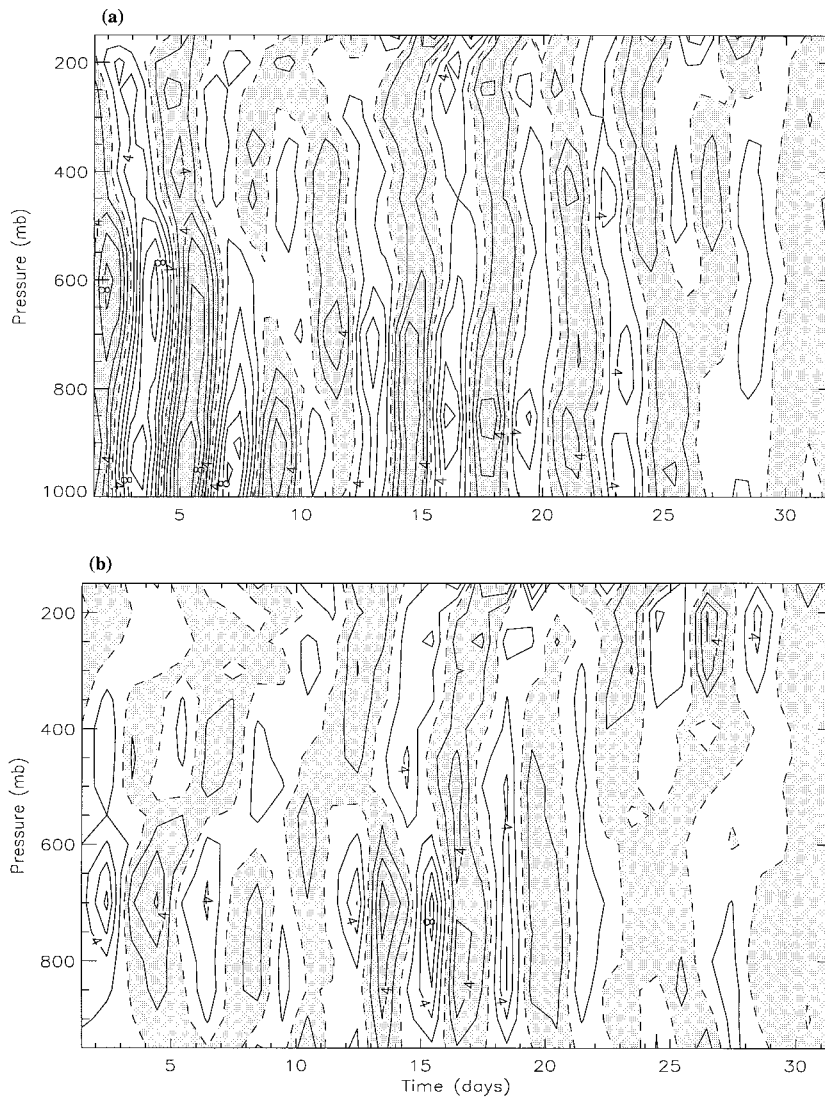


FIG. 7. Time–height sections of 2.5–6-day bandpass-filtered meridional wind from radiosonde data at (a) Dakar and (b) Bamako in Jul 1995. Contour interval = 2 m s⁻¹. Shaded regions correspond to northerlies from radiosonde data.

series filtered between 2.5 and 6 days was 25.0 and 39.4 at Dakar and Bamako, respectively. Hence, stronger convective activity was associated with the waves that passed over Bamako.

The analysis of the radiosonde data and the satellite imagery showed big differences between Dakar and Bamako. These differences reflect the complicated structure of the AEWs, consistent with the discussion in the introduction. Therefore, AEWs cannot simply be viewed as sinusoidal waves at 700 mb in the rainy zone since significant amplitudes are also apparent at low levels north of the jet. The idea that the significant low-level amplitudes observed at Dakar can be attributed to AEWs growing to the north of the AEJ will be elaborated on in the following section using UKMO analysis data.

b. UKMO analyses

The single-point analysis (using radiosonde data) has provided an indication of the characteristics of the AEWs in 1995. However, a broader-scale picture of the easterly waves will be obtained from an examination of the UKMO model analyses.

1) POWER SPECTRA

Power spectrum analysis of meridional and zonal wind time series at 950 and 700 mb at two grid points close to the actual location of Dakar and Bamako has been performed in order to confirm the existence and periodicity of the AEWs in the model analyses. The

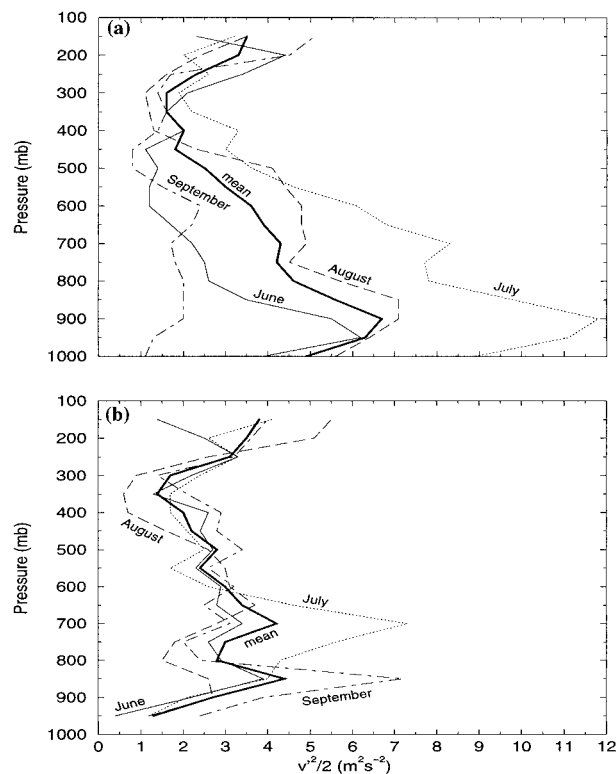


FIG. 8. Graphs of the mean $v'^2/2$ (v' is the 2.5–6-day bandpass-filtered meridional wind) vs height (a) for Dakar in 1995, (b) for Bamako in 1995. Solid line: Jun, dotted line: Jul, dashed line: Aug, dot-dashed line: Sep, and bold solid line: the mean for the Jun–Sep period (radiosonde data).

coordinates of the two selected points are 14.583°N , 16.875°W and 12.083°N , 6.875°W (Fig. 5). Spectral peaks between 2.5- and 5-day periods appeared at both grid points (Fig. 9). In the zonal wind component, u , the variations were almost always stronger in the grid point near Dakar except in the daily timescale (Figs. 9a,c). In the meridional wind component, v , the results were similar to the radiosonde data as expected. Stronger spectral energy associated with AEWs was observed at very low levels in the grid point near Dakar (Fig. 9d), while at 700 mb (Fig. 9b) the stronger spectral peak associated with AEWs was observed near Bamako, consistent with the radiosonde data. It is interesting to note the strong signal of the diurnal cycle that appeared at low levels in the grid point near Bamako (Figs. 9c,d) and also that strong oscillations in the 700-mb u and v time series (Figs. 9a,b) were observed in periods of about 8 days. Viltard and De Felice (1979) had also found strong variance at around 7.5 days on the meridional wind at Dakar. Further analysis of the 8-day signal is beyond the scope of this study.

2) MERIDIONAL DIFFERENCES AND LONGITUDINAL VARIATION OF AEW STRUCTURES

The existence of two regions of AEW development on either side of the AEJ is further illustrated in Fig.

10, using the July–September time-mean value of the quantity $0.5(u'^2 + v'^2)$ (u' , v' are the 2.5–5-day filtered winds) at 950 and 700 mb, as well as the mean location of the AEJ (averaged from July to September 1995). Figure 10a clearly shows that at 700 mb the waves attain maximum amplitude south of the AEJ where a double maximum appears near the West African coast in agreement with Albignat and Reed (1980). At very low levels and particularly at 950 mb (Fig. 10b) the maximum amplitude is observed on the northern flank of the jet where the sub-Saharan baroclinic zone exists. Strong wave amplitudes are also observed just off the coast south of the land maximum. At 850 mb (not shown) both tracks—north and south of the AEJ—can be seen. As far as the genesis of the waves is concerned, they appear in the analyses at 700 mb to attain energy stronger than $2 \text{ m}^2 \text{ s}^{-2}$ at about $10^\circ\text{--}15^\circ\text{E}$ in the rainy zone of Africa while at 950 mb these amplitudes are reached between about $0^\circ\text{--}5^\circ\text{E}$ in the sub-Saharan baroclinic zone. The identification of these areas as the most probable regions for the initial development of the AEWs is in good agreement with Reed et al. (1988a,b).

Figure 10 clearly confirms the idea (presented in section 1) that AEWs are not only expected to form in the southern flank of the jet near the AEJ level (because of the interactions between the opposite sign PV gradients) but also on its northern flank in association with the strong low-level θ gradients and low static stability there. These low-level waves (on the northern flank of the AEJ) were responsible for the large values of meridional wind variance observed at Dakar at low levels (see Fig. 8a). The extension of the 950-mb maximum over the ocean south of the inland maximum suggests that the low-level waves continue to move southwestward when they meet the coast as suggested by Reed et al. (1988a,b; Fig. 1a), although one must bear in mind that part of the 950-mb amplitude over the ocean could be attributed to downward development of the 700-mb waves near the coast.

An examination of horizontal charts of the mean value of the quantity $0.5(u'^2 + v'^2)$ for each month (not shown) showed seasonal variation in the magnitude and location of the AEWs at these two levels. At 950 mb, stronger energy was observed in July (near the coast) and the maximum was located more equatorward than later in the season. At 700 mb, the energy maximum was strongest in August. At this level two maxima (over the land and just off the coast) appeared during the season. The large values of energy observed in August at 700 mb are consistent with the finding that stronger negative meridional PV gradients were observed in August (section 3).

The evolution of the AEWs as they propagate along the AEJ will now be considered. Figure 11 contains latitude–time diagrams of 2.5–5-day filtered meridional wind at different longitudes. In Fig. 11 the bold line is a 15-day moving average of the latitude of the maximum

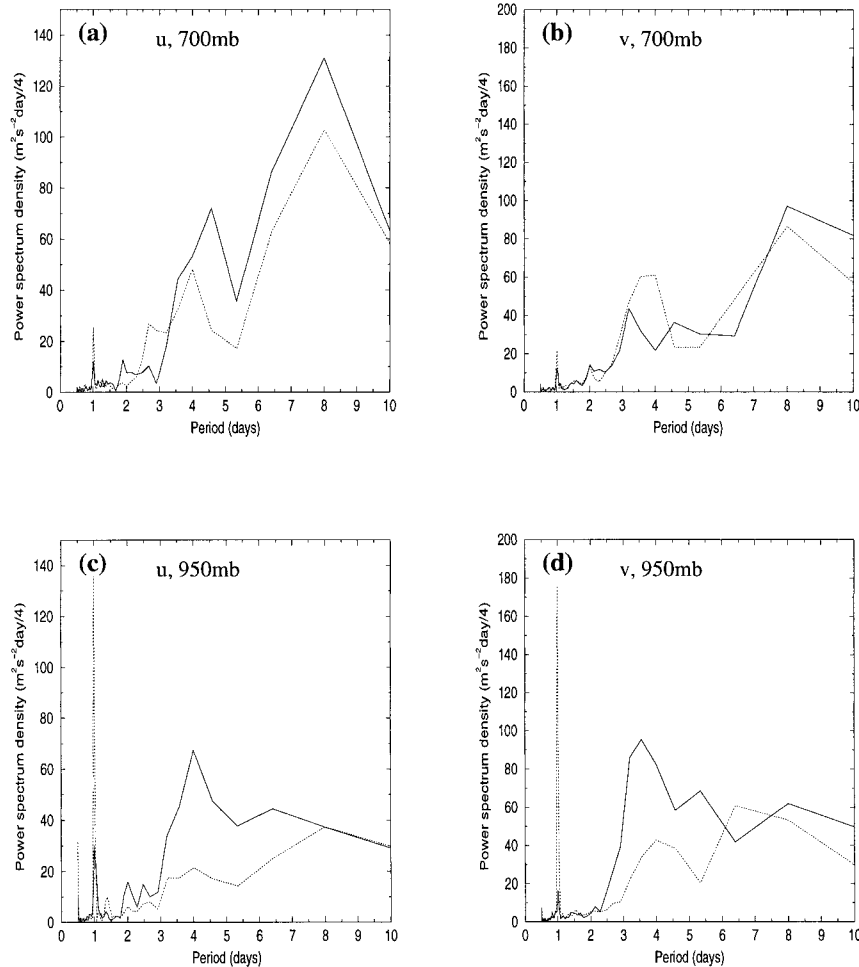


FIG. 9. Power spectrum density vs period of (a) zonal wind at 700 mb, (b) meridional wind at 700 mb, (c) zonal wind at 950 mb, and (d) meridional wind at 950 mb at 14.583°N, 16.875°W (solid line), 12.083°N, 6.875°W (dotted line) (UKMO analysis data).

easterly flow (between 5° and 20°N) at any longitude at 700 mb and corresponds to the latitude of the AEJ.

At 5.625°E the activity is clearly stronger at 700 mb south of the jet (Fig. 11a). At 950 mb (Fig. 11b) there are only a few weak waves. The indication that the waves are better developed at 700 mb south of the jet than at lower levels at 5.625°E is consistent with Fig. 10. As the waves propagate westward their amplitude increases and at 4.375°W (Figs. 11c,d) it can be seen that strong waves exist on both sides of the jet. At 700 mb (Fig. 11c) the maximum wave amplitude is either at the jet latitude or south of it, while at 950 mb (Fig. 11d) the waves are clearly defined north of the jet latitude. At 9.375°W (Figs. 11e,f) the situation is very similar. An interesting feature that appears at this longitude is the latitudinal migration of the wave activity with the jet. Early in July the jet maximum was located at about 13°N and the wave activity was concentrated very close to the AEJ maximum at 700 mb and about 5° to the north at 950 mb. As the season progressed the

wave activity migrated more to the north and later it returned southward confirming a close link between waves and jet. This migration of the wave activity with time is even clearer in Fig. 11f (which shows the waves at 950 mb) because the low-level waves attain maximum amplitude at these longitudes. As the waves approach the West African coast their tracks begin to converge (Figs. 11g,h). The wave structure becomes deeper and stronger winds appear at low levels south of the jet. Finally, over the ocean at 24.375°W (Figs. 11i,j) there is no clear separation between waves in the northern and southern flank of the 700-mb jet. More and generally stronger structures appear at 700 mb (Fig. 11i).

As a final comment it must be mentioned that an interesting and consistent feature throughout western Africa is that the waves appear in packets of about three waves (e.g., Figs. 11e,f). A possible reason for this may have to do with changes in the strength and associated instability of the AEJ, with periods of strong wave activity and a weakening of the jet, followed by low wave

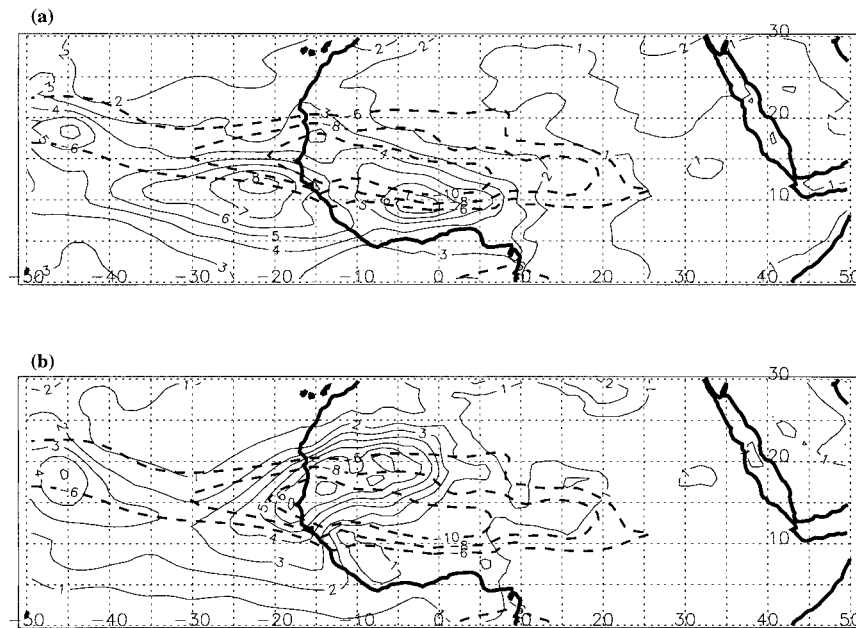


FIG. 10. Mean $(u'^2 + v'^2)/2$ ($\text{m}^2 \text{s}^{-2}$) averaged from Jul to Sep 1995 at (a) 700 mb and (b) 950 mb. Here u' , v' are the 2.5–5-day bandpass-filtered zonal and meridional winds. Contour interval = $1 \text{ m}^2 \text{ s}^{-2}$. The bold dashed contours show regions where the mean easterly flow at 700 mb (from Jul to Sep 1995) was stronger than 6 m s^{-1} . Contour interval = 2 m s^{-1} (UKMO analysis data).

activity while the jet replenishes its strength (cf. Thorncroft and Blackburn 1999). In any case, the existence of packets of about three waves may also be consistent with the 8-day peak in the power spectrum of the 700-mb wind.

The existence of AEWs exhibiting maximum amplitude below the AEJ level and growing on the poleward side of the AEJ has been confirmed. A remaining very interesting question that was also posed by Nitta and Takayabu (1985) is whether these waves evolve in isolation of the 700-mb waves (south of the jet) or if they are part of the same AEW. Cross correlations between 2.5- and 5-day meridional wind time series at different latitudes and longitudes were calculated in order to examine whether there is coherence between the waves following the two tracks. For brevity only the results obtained at 4.375°W will be shown. This longitude was chosen because the waves on both sides of the jet are well developed there. Similar results were obtained from cross correlations made at other longitudes (not shown). Figure 12 presents the cross correlations between the time series at 9.583°N at 700 mb and at (a) 9.583°N , (b) 14.583°N , (c) 19.583°N at 950 mb. The 9.583°N lat was chosen as reference latitude for the 700-mb flow at the above-mentioned longitude because the waves exhibit maximum amplitude at 700 mb over land there (see Fig. 10a). Negative lag means that the 700-mb wave is behind (i.e., east of) the 950-mb one.

The maximum correlation at 4.375°W is equal to about 0.83 and it is observed for lag = -0.25 days

between the time series at 9.583°N (700 mb) and at 14.583°N (950 mb) (Fig. 12). This also implies an eastward tilt with height consistent with baroclinic growth. Even at higher latitudes (e.g., at 19.583°N) the correlation remains high (Fig. 12). Similar lag correlations at other longitudes (not shown) suggest that there is a separation of about 5° – 6° lat between the 700-mb and the low-level waves throughout western Africa. Over the ocean this separation becomes almost 0° ; that is, the 700-mb meridional wind time series are strongly correlated with the 950-mb ones only for nearby latitudes.

The cross-correlation analysis suggests that there is a high degree of coherence between the 700-mb waves south of the AEJ and the low-level waves north of the jet. This important result confirms the complicated structure of the AEWs. The 700-mb and the low-level waves are not independent structures but are part of the same AEW. An interesting topic for future work is to examine whether the two parts of the AEW grow simultaneously or if one part dominates in individual waves.

3) ENERGETICS INFERRED FROM FILTERED COVARIANCES

Burpee (1972) found that both baroclinic and barotropic instability are important for the growth of the AEWs. To assess qualitatively the relative importance of these two mechanisms for the growth of the 700-mb and low-level structures the $\omega'T'$, $v'T'$, $u'v'$ covari-

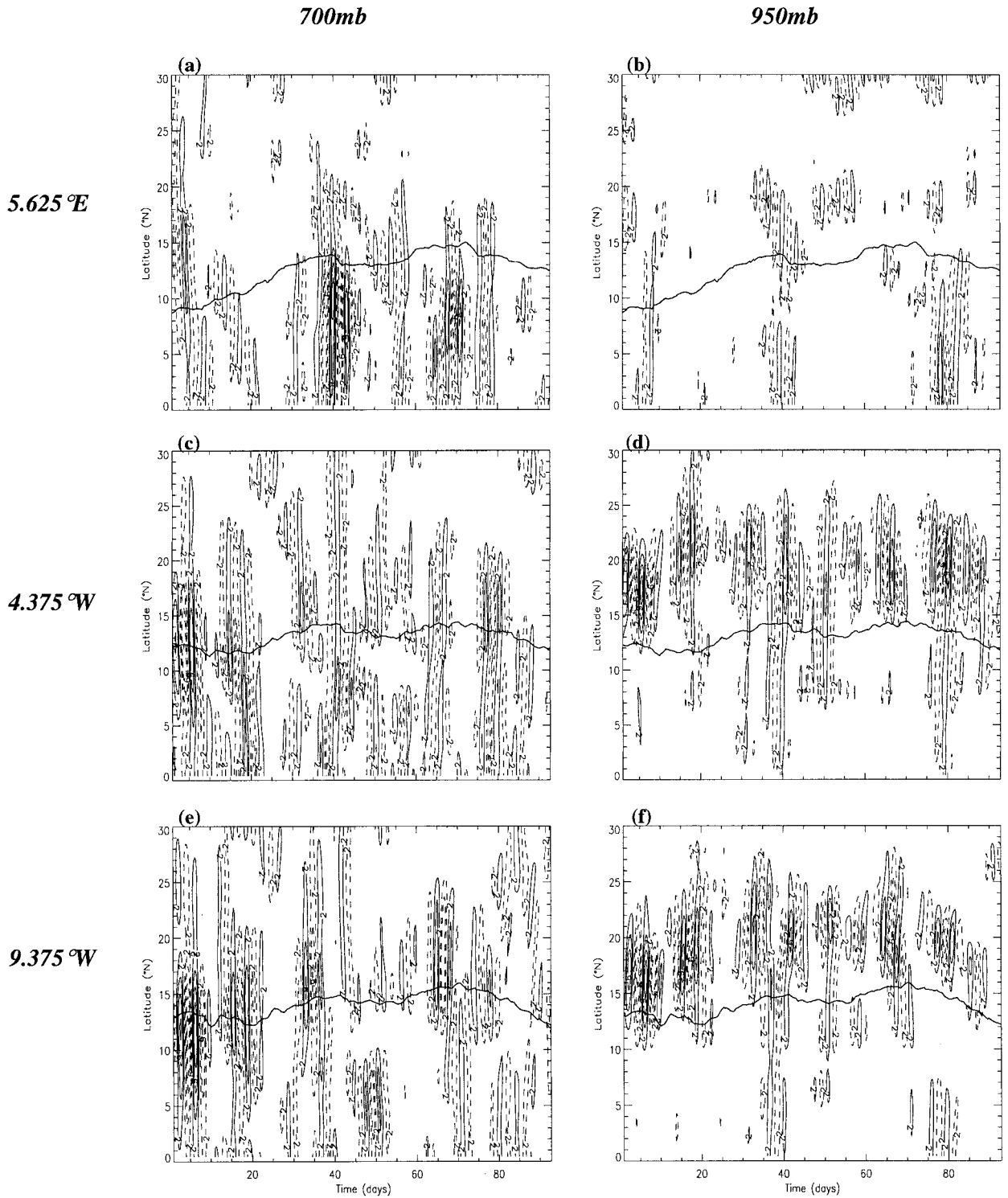


FIG. 11. Latitude–time diagrams of 2.5–5-day period meridional wind (m s^{-1}) from Jul to Sep 1995 at (a,b) 5.625°E, (c,d) 4.375°W, (e,f) 9.375°W, (g,h) 18.125°W, (i,j) 24.375°W. Left column: 700 mb, right column: 950 mb. Contour interval = 2 m s^{-1} . Dashed lines correspond to northerlies. The location of the AEJ is indicated by the bold line. See text for details (UKMO analysis data).

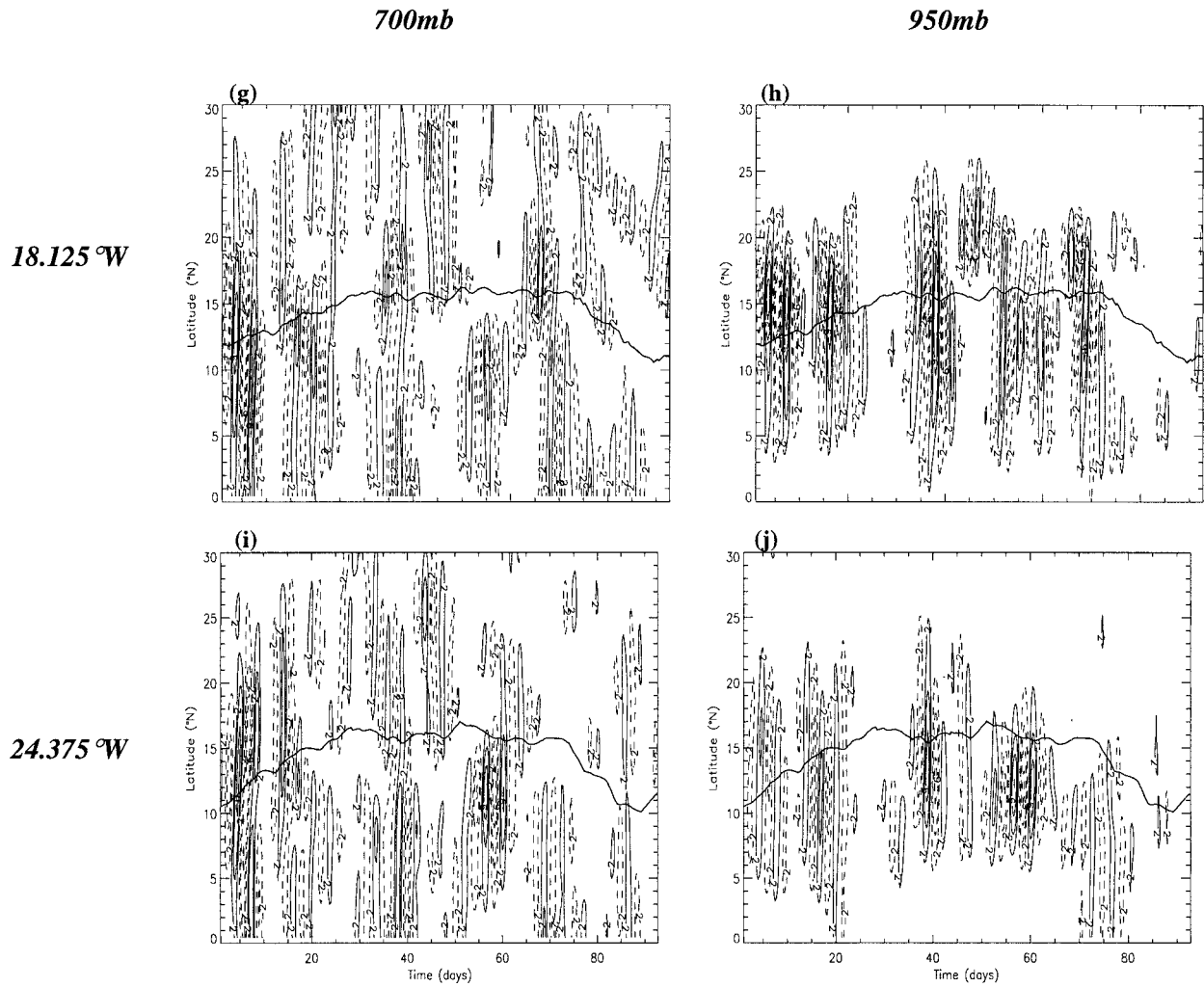


FIG. 11 (Continued)

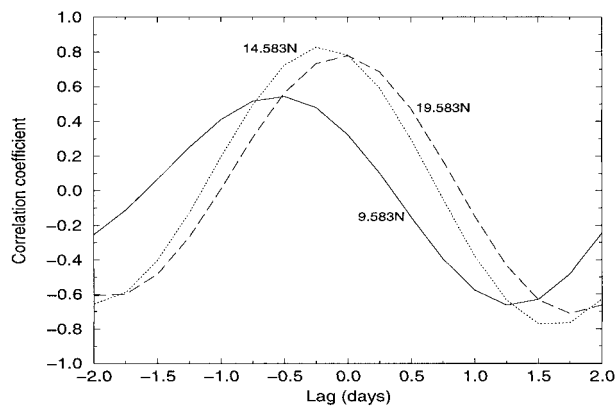


FIG. 12. Cross correlations at 4.375°W between the 2.5–5-day bandpass-filtered meridional wind time series at 9.583°N at 700 mb and at 9.583°N (solid), 14.583°N (dotted), and 19.583°N (dashed) at 950 mb. Positive lag means that the 950-mb time series lags behind the 700-mb time series (UKMO analysis data).

ances have been calculated. Bandpass filtering in the 2.5–5-day timescale at 950 mb, 850 mb, and 700 mb was performed in u , v , ω ($=dp/dt$), and temperature (T) in order to calculate these covariances. Through the calculation of the covariances it is not intended to provide a strict analysis of the energetics of the waves, but to examine the geographical distribution of the conversion terms (in the Lorenz energetics diagram). This approach was previously followed by Albignat and Reed (1980) and Reed et al. (1988b).

The $\overline{\omega'T'}$ covariance exhibits largest values slightly north of the mean latitude of the jet with a maximum at about 16°N , 5°W at 850 mb (Fig. 13a). The high values at 850 mb extend from about 5°E to $20^{\circ}\text{--}25^{\circ}\text{W}$ (i.e., just off the coast). The sign of this covariance indicates a conversion of eddy available potential energy (AE) to eddy kinetic energy (EKE). Similarly, the $\overline{v'T'}$ covariance exhibits highest values just north of

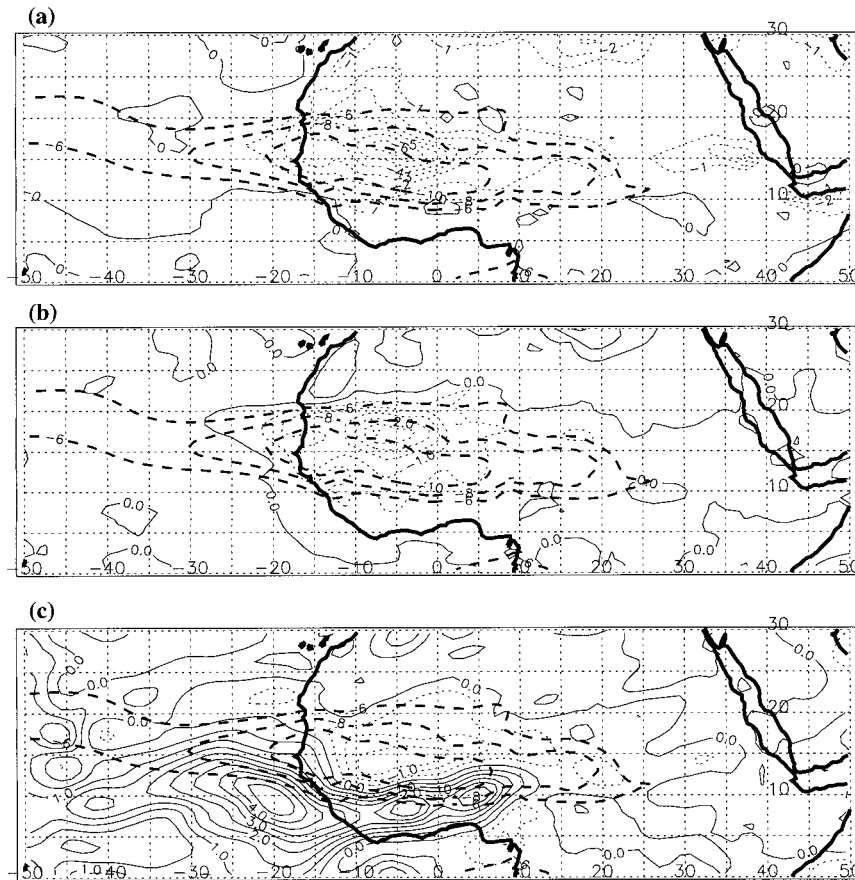


FIG. 13. Covariances (from Jul to Sep 1995) for the 2.5–5-day period of (a) omega and temperature (10^{-2} Pa s^{-1} K) at 850 mb, (b) meridional wind and temperature ($m s^{-1}$ K) at 950 mb, and (c) of zonal and meridional winds ($m^2 s^{-2}$) at 700 mb. Contour interval: 1, 0.5, 0.5, respectively. The bold dashed contours show regions where the mean easterly flow at 700 mb (from Jul to Sep 1995) was stronger than $6 m s^{-1}$. Contour interval = $2 m s^{-1}$ (UKMO analysis data).

the mean latitude of the jet (Fig. 13b) and a maximum at 950 mb (at about $17^{\circ}N$, $8^{\circ}W$). The sign of the covariance in association with the strong positive meridional temperature gradient that is observed there (Fig. 5) implies a conversion of zonal available potential energy to AE. On the other hand, the $\overline{u'v'}$ covariance at 700 mb (Fig. 13c)—which is the level where it attains maximum values—is positive south of the jet and negative to the north. Higher values are observed south of the jet and especially over the ocean. The sign of the $\overline{u'v'}$ covariance on either side of the jet (at 700 mb) in conjunction with the meridional gradient of the zonal wind (Fig. 13c) implies a conversion of zonal kinetic energy to EKE on both sides of the jet. Hence, it is concluded that the low-level waves on the northern side of the jet grow mainly from the baroclinic energy conversion (which has larger values at low levels) while south of the jet the barotropic energy conversion dominates [in agreement with Norquist et al. (1977)] and the maximum energy input in the waves is at 700 mb.

c. Discussion

Based on the results in this section the life cycle of a typical AEW can be envisaged. It must be mentioned that this study is based on data from one year only and interannual variations are certainly expected. Initially the easterly wave disturbances seem to appear at 700 mb (close to the jet latitude) at about 10° – $15^{\circ}E$. It is possible, however, that some disturbances originate farther east but do not attain significant strength until they reach the above longitudes (cf. Burpee 1972; Carlson 1969a).

Because of the strong momentum fluxes on the equatorward side of the jet (Fig. 13c), the AEWs gain much energy there (i.e., they grow barotropically), and they are well detected before they cross the prime meridian, in contrast to the waves to the north. The meridional gradient of PV is stronger on the southern flank of the jet and it remains almost unchanged from about $20^{\circ}E$ until the coast. The low-level structures develop only when the wave reaches the regions where the $\partial\theta/\partial y$

gradients are strong and the static stability is low. The interaction between the jet-level PV gradients and the low-level θ gradients is assisted by the low dry static stability that exists on the poleward side of the jet in association with the very deep well-mixed boundary layer. At the same time the 700-mb wave amplitude increases and some identification of this wave at low levels (i.e., below the 700-mb maximum) occurs only near the coast probably in association with latent heating. Hence, the AEWs grow through a mixed barotropic–baroclinic instability (Burpee 1972; Thorncroft and Hoskins 1994a) with barotropic instability acting initially.

The 700-mb wave that has maximum amplitude near the jet core and generally on the southern flank exhibits strong coherence with the low-level waves to the north. However, the former wave propagates on the PV gradients that exist from the rainy zone of North Africa until Central America (Fig. 4), while the latter waves propagate on the θ gradients (Fig. 5) that exist only on the southern flank of the Saharan Desert.

In section 3 it was mentioned that when the low-level AEWs encounter the West African coast there are three possibilities. From the results presented in this study the most probable track appears to be the southwestward track as found by Reed et al. (1988a). Finally, either if the low-level waves merge with the 700-mb ones creating a deep structure or if they continue to move in isolation, they must be taken into account since their energy is concentrated at very low levels, which could make them likely candidates for precursors of tropical cyclones. Indeed, Karyampudi et al. (1997) found that a low-level vortex of unknown origin, which was advected from the north was associated with the genesis of Tropical Storm Ernesto in 1994 at about 10.1°N, 29.9°W. Also, Lawrence et al. (1998) noticed that the wave that formed Tropical Storm Chantal in 1995 crossed the West African coast on 5 July and soon showed signs of a low-level circulation. This wave can be seen to exhibit a strong signal at low levels at Dakar (see Fig. 7a).

5. Conclusions

The existence of low-level easterly wave structures to the north of the AEJ has been shown. Radiosonde data analysis showed that waves with AEW periods and maximum amplitudes at low levels pass Dakar. The vertical distribution of the wave amplitude was different in Bamako where the typical 700-mb waves were encountered. These results were also verified by the UKMO global model analyses. The model analyses exhibited strong low-level amplitudes—associated with 2.5–5-day easterly waves—on the northern flank of the AEJ where the low-level waves are expected to form. These strong low-level amplitudes extended for about 15° over the ocean displaced south of the land maxi-

mum. On the other hand, strong 700-mb amplitudes appear in the southern flank of the jet.

The low static stability and the temperature gradients on the southern flank of the Sahara are conducive for the development of the low-level waves north of the jet. These waves develop in association with the interactions of the negative meridional PV gradients that exist in the jet core with the low-level θ gradients. It is suggested that baroclinic instability is mainly responsible for the maintenance and development of the low-level waves to the north, consistent with the theory that predicts larger amplitude baroclinic disturbances in the low-dry-static-stability region north of the jet (Chang 1993; Thorncroft 1995). The convective activity associated with these waves is weaker than that of the waves that propagate in the rainy zone of North Africa.

Although there are some differences between the low-level and the 700-mb waves, it was found that they constitute a single mode and propagate simultaneously at least over the African continent. The former waves propagate westward following the θ gradients over land, while their 700-mb counterparts follow the PV gradients not only over the land but also over the ocean. This confirms that the AEWs are complicated structures composed of two circulation centers, one at low levels north of the jet and the other at the jet level. Finally, more attention should be given to the low-level structures north of the jet since some of them move over the ocean and could be associated with tropical cyclogenesis.

Acknowledgments. We would like to thank Ed Dicks for his assistance with programming as well as John Molinari and two anonymous reviewers for their helpful comments. This work was funded by European Commission Grant ERBFMBICT961444.

REFERENCES

- Albignat, J. P., and R. J. Reed, 1980: The origin of African wave disturbances during phase III of GATE. *Mon. Wea. Rev.*, **108**, 1827–1839.
- Avila, L. A., and R. J. Pasch, 1995: Atlantic tropical systems of 1993. *Mon. Wea. Rev.*, **123**, 887–896.
- Burpee, R. W., 1972: The origin and structure of easterly waves in the lower troposphere of North Africa. *J. Atmos. Sci.*, **29**, 77–90.
- , 1974: Characteristics of the North African easterly waves during the summers of 1968 and 1969. *J. Atmos. Sci.*, **31**, 1556–1570.
- Carlson, T. N., 1969a: Synoptic histories of three African disturbances that developed into Atlantic hurricanes. *Mon. Wea. Rev.*, **97**, 256–276.
- , 1969b: Some remarks on African disturbances and their progress over the tropical Atlantic. *Mon. Wea. Rev.*, **97**, 716–726.
- Chang, C. B., 1993: Impact of desert environment on the genesis of African wave disturbances. *J. Atmos. Sci.*, **50**, 2137–2145.
- Charney, J. G., and M. E. Stern, 1962: On the stability of internal baroclinic jets in a rotating atmosphere. *J. Atmos. Sci.*, **19**, 159–172.
- Cullen, M. J. P., 1993: The Unified Forecast/Climate model. *Meteor. Mag.*, **122**, 81–94.

- Duchon, C. E., 1979: Lanczos filtering in one and two dimensions. *J. Appl. Meteor.*, **18**, 1016–1022.
- Emanuel, K. A., 1986: An air–sea interaction theory for tropical cyclones. Part I: Steady-state maintenance. *J. Atmos. Sci.*, **43**, 585–604.
- Frank, N. L., 1970: Atlantic tropical systems of 1969. *Mon. Wea. Rev.*, **98**, 307–314.
- Hoskins, B. J., M. E. McIntyre, and A. W. Robertson, 1985: On the use and significance of isentropic potential vorticity maps. *Quart. J. Roy. Meteor. Soc.*, **111**, 877–946.
- Karyampudi, V. M., J. Simpson, S. Palm, and H. Pierce, 1997: Lidar observations of Saharan dust layer and its influence on tropical cyclogenesis. Preprints, *22d Conf. on Hurricanes and Tropical Meteorology*, Ft. Collins, CO, Amer. Meteor. Soc., 59–60.
- Landsea, C. W., 1993: A climatology of intense (or major) Atlantic hurricanes. *Mon. Wea. Rev.*, **121**, 1703–1713.
- , W. M. Gray, P. W. Mielke Jr., and K. J. Berry, 1994: Seasonal forecasting of Atlantic hurricane activity. *Weather*, **49**, 273–284.
- Lawrence, M. B., B. M. Mayfield, L. A. Avila, R. J. Pasch, and E. N. Rappaport, 1998: Atlantic hurricane season of 1995. *Mon. Wea. Rev.*, **126**, 1124–1151.
- Miyakoda, K., J. Sheldon, and J. Sirutis, 1982: Four-dimensional analysis experiment during the gate period. Part II. *J. Atmos. Sci.*, **39**, 486–506.
- Molinari, J., S. Skubis, and D. Vollaro, 1995: External influences on hurricane intensity. Part III: Potential vorticity structure. *J. Atmos. Sci.*, **52**, 3593–3606.
- , D. Knight, M. Dickinson, D. Vollaro, and S. Skubis, 1997: Potential vorticity, easterly waves, and eastern Pacific tropical cyclogenesis. *Mon. Wea. Rev.*, **125**, 2699–2708.
- Nitta, T., and Y. Takayabu, 1985: Global analysis of the lower tropospheric disturbances in the Tropics during the northern summer of the FGGE year. Part II: Regional characteristics of the disturbances. *Pure Appl. Geophys.*, **123**, 272–292.
- Norquist, D. C., E. E. Recker, and R. J. Reed, 1977: The energetics of African wave disturbances as observed during phase III of GATE. *Mon. Wea. Rev.*, **105**, 334–342.
- Paradis, D., J. P. Lafore, J. L. Redelsperger, and V. Balaji, 1995: African easterly waves and convection. Part I: Linear simulations. *J. Atmos. Sci.*, **52**, 1657–1679.
- Pasch, R. J., L. A. Avila, and J.-G. Jiing, 1998: Atlantic tropical systems of 1994 and 1995: A comparison of a quiet season to a near-record-breaking one. *Mon. Wea. Rev.*, **126**, 1106–1123.
- Reed, R. J., D. C. Norquist, and E. E. Recker, 1977: The structure and properties of African wave disturbances as observed during phase III of GATE. *Mon. Wea. Rev.*, **105**, 317–333.
- , A. Hollingsworth, W. A. Heckley, and F. Delsol, 1988a: An evaluation of the ECMWF operational system in analyzing and forecasting easterly wave disturbances over Africa and the tropical Atlantic. *Mon. Wea. Rev.*, **116**, 824–865.
- , E. Klinker, and A. Hollingsworth, 1988b: The structure and characteristics of African easterly wave disturbances as determined from the ECMWF Operational Analysis/Forecast System. *Meteor. Atmos. Phys.*, **38**, 22–33.
- Riehl, H., 1954: *Tropical Meteorology*. McGraw-Hill, 392 pp.
- Thorncroft, C. D., 1995: An idealized study of African easterly waves. Part III: More realistic basic states. *Quart. J. Roy. Meteor. Soc.*, **121**, 1589–1614.
- , and B. J. Hoskins, 1994a: An idealized study of African easterly waves. Part I: A linear view. *Quart. J. Roy. Meteor. Soc.*, **120**, 953–982.
- , and —, 1994b: An idealized study of African easterly waves. Part II: A nonlinear view. *Quart. J. Roy. Meteor. Soc.*, **120**, 983–1015.
- , and M. Blackburn, 1998: Maintenance of the African Easterly Jet. *Quart. J. Roy. Meteor. Soc.*, **125**, 763–786.
- Viltard, A., and P. De Felice, 1979: Statistical analysis of wind velocity in an easterly wave over West Africa. *Mon. Wea. Rev.*, **107**, 1320–1327.